A Multi-Strategy Adaptive Error Modeling and Compensation Method for Star Point Centroid Extraction

Yifan Lou[1]*, Mi Wang[1], Tiyou Zhou[1], Haonan Zhang[1], Huang Zhang[2]

[1]State Key Laboratory of information Engineering in Surveying, Mapping and Remote Sensing(LIESMARS), Wuhan University, Wuhan 430072, China

[2]Hubei Subsurface Multi-scale Imaging Key Laboratory, School of Geophysics and Geomatics, China University of Geosciences, Wuhan, 430074, China

Keywords: Centroid extraction, Error compensation, Adaptive strategy, Unscented Kalman filter, Subpixel interpolation.

Abstract:

Centroid extraction from star images is a critical component in achieving high-precision satellite attitude determination. Prevailing approaches primarily focus on suppressing a single type of error or depend on fixed filtering and compensation parameters, often lacking a multidimensional and fine-grained analysis and handling of diverse error sources. To address these limitations, this paper proposes a compensation method for centroid extraction based on error classification and modeling, coupled with an adaptive strategy selection mechanism to improve accuracy. Experimental results demonstrate the efficacy of the proposed method: on a set of 30 to 300 laboratory-simulated star images, it enhanced the average centroid extraction accuracy from a baseline of 0.31–0.45 pixels to 0.11–0.19 pixels when using a Static model Unscented Kalman Filter (UKF) integrated with four sub-pixel interpolation techniques. Furthermore, for a larger dataset of 300 to 600 star images simulated at a 300 Hz frame rate, the method achieved an accuracy improvement exceeding 50% across five different motion model UKF methods, demonstrating robust performance.

1. Introduction

Star trackers are currently the most precise devices for absolute attitude measurement in spacecraft, with the centroid extraction of stellar images serving as the foundation for their attitude determination (Liebe et al., 2002). Increasingly stringent requirements for satellite attitude determination and control in fields such as high-precision astronomical observation, deep-space exploration, and high-accuracy Earth observation have raised new challenges for centroid extraction, particularly with the demand for sub-arcsecond-level attitude accuracy (Sun et al., 2013). Consequently, advancing high-precision star image centroid extraction and error compensation techniques has become a critical prerequisite for enhancing the autonomous navigation capability and observational performance of spacecraft, carrying significant theoretical value and urgent engineering relevance (Jiang et al., 2016).

Centroid extraction is a classical problem of estimating the position of a continuous energy distribution from discrete digital measurements. Its error sources are diverse and span the entire processing chain—from optical system aberrations and sensor noise to subsequent image-processing algorithms (Yu et al., 2023). Traditional centroid extraction algorithms, such as the center-of-gravity method (Tjorven et al., 2013) and the squared-gray-level centroid method (Shortis et al., 1994), rely on intensity-weighted distance metrics. Although simple and computationally efficient, these approaches struggle to capture and model the coupling mechanisms and propagation characteristics of various errors introduced during the discretization and sampling of stellar intensity distributions. Wei et al. proposed a method for compensating systematic errors in centroid extraction using frequency-domain analysis and numerical simulation, which improved stellar centroid prediction accuracy (Wei et al., 2019). However, deep learning-based approaches depend heavily on extensive annotated datasets and specific training samples, limiting their generalizability across different sensor configurations and operating conditions.

As star sensors increasingly target fainter and higher-frequency objects and become more prevalent on constrained platforms such as microsatellites, a multitude of centroid extraction methods have emerged (Bin et al., 2016). In the context of highly dynamic and complex environments, Zong et al. developed an algorithm based on edge detection and pixel filtering, applicable under strong interference conditions (Zong et al., 2014). Wang et al. proposed a multi-step method based on minimum energy difference, improving centroid extraction accuracy in near-infrared star images under low signal-to-noise ratio (SNR) conditions (Wang et al., 2013). Other studies have focused on refining the centroid extraction algorithm itself to enhance accuracy and noise resistance. For example, Luo et al. proposed an improved star sensor centroid extraction algorithm that adjusts pixel grayscale values based on the energy distribution characteristics of star points, achieving higher extraction accuracy with lower computational complexity (Luo et al., 2015). Nonetheless, a critical issue that remains unresolved is how to adaptively select the optimal compensation strategy based on real-time characteristics of star images—such as signal-to-noise ratio, local curvature, and star motion state—rather than relying on fixed processing workflows (Tan et al., 2017). Despite numerous accomplishments by researchers worldwide in star point centroid extraction, current studies still exhibit gaps and controversies. Most research focuses on suppressing a single type of error or relies on fixed filtering and compensation parameters, lacking multidimensional and adaptive processing of error sources.

Based on the above analysis, this paper proposes an error decomposition and compensation framework that integrates the unscented Kalman filter (UKF) motion model with sub-pixel interpolation. The framework performs a refined decomposition of centroid extraction errors across three dimensions: systematic low-frequency errors, high-frequency random errors, and model errors. Concurrently, a multi-strategy adaptive error compensation scheme is designed to comprehensively improve centroid extraction accuracy.

2. Method

The methodology presented in this paper comprises the following key steps:

1. True Value Establishment and Spatio-Temporal Filtering;
2. Error Models and Decomposition;
3. Multi-Strategy Error Compensation Methods;
4. Adaptive Selection Mechanism for Error Compensation Strategies;
5. Evaluation Criteria.

2.1 True Value Establishment and Spatio-Temporal Filtering

The proposed centroid extraction methodology comprises image preprocessing, sub-pixel refinement, and spatio-temporal filtering.

Initially, star regions are localized through denoising, background estimation, and foreground extraction. Candidate points are screened using connected component analysis and morphological operations. During refinement, second-order Gaussian fitting provides coarse localization, followed by sub-pixel interpolation methods to calculate precise coordinates.

We then transition from single-frame spatial processing to spatio-temporal tracking by introducing an Unscented Kalman Filter to filter the trajectories. This is necessitated by the high-frequency nature of our observational data, specifically sampled at 200 Hz and 300 Hz. At these frame rates, trajectories contain high-frequency sensor noise and complex, non-linear micro-vibrations from the platform. Traditional single-frame algorithms cannot suppress these dynamic noises. Unlike the Extended Kalman Filter, which suffers from Jacobian approximation errors, the Unscented Kalman Filter accurately handles non-linear dynamics. Its predict-update mechanism smoothly tracks the trajectory while rejecting transient spatial outliers.

Finally, the brightest star point in each image is selected to construct a continuous centroid sequence. We establish the global mean of this sequence as the ground truth to rigorously evaluate extraction accuracy. This approach relies on strict physical and statistical principles. Physically, our laboratory calibration utilizes a static staring observation setup, meaning the true focal-plane position of the star spot is fixed. Inter-frame centroid fluctuations are thus primarily induced by zero-mean random noise and platform jitter. Statistically, the Law of Large Numbers dictates that the global mean of an extensive high-frequency sample sequence converges to the best linear unbiased estimator of the true coordinate. In the absence of external absolute metrology, this global mean serves as the most reliable statistical ground truth.

2.2 Error Models and Decomposition

The errors in star centroid extraction are analyzed and decomposed into three dimensions: systematic low-frequency errors, high-frequency random errors, and model errors. Systematic errors are mainly induced by hardware and environmental factors, typically characterized by low-frequency drift or periodic vibration, which are reflected in error accumulation over prolonged durations. Random errors, originating from measurement noise and inherent instrument inaccuracies, present as irregular fluctuations. Model errors, on the other hand, indicate a discrepancy between the employed measurement model and the actual physical system, usually caused by model simplification or unaccounted-for factors.

2.3 Multi-Strategy Error Compensation Methods

To effectively address the three aforementioned error categories, we propose a framework comprising five distinct compensation algorithms, deployed as follows:

1.Systematic Low-Frequency Errors:

Adaptive Window Trend Estimation Algorithm;

Confidence-Weighted Truth Value Correction Algorithm.

2.High-Frequency Random Errors:

Adaptive Median Filtering Algorithm for Windows;

Local Trajectory Smoothing Algorithm.

3.Model Errors:

Error Prediction Compensation Algorithm Based on AR Models;

Confidence-Weighted Truth Value Correction Algorithm.

2.3.1 Adaptive Window Trend Estimation Algorithm

This paper proposes a moving average method based on adaptive windows for extracting trend components from data. The computational steps are as follows:

Step1:

Extract the noise level from error analysis and calculate the signal-to-noise ratio (SNR) based on the maximum value and standard deviation.

Step 2:

Dynamically calculate the filter window size: Adjust the window size based on noise intensity. The window size W ranges from 3 to 11, taking odd values to accommodate varying noise levels.

Step 3:

Compute the trend estimate using a sliding window averaging method. Subtract the trend estimate from each observation to obtain the compensated observation.

The window size W is dynamically adjusted based on the dominant error frequency f_d. The window size is inversely proportional to the frequency, as expressed by the following formula:

$$W = \lfloor \frac{f_s}{2f_d} \rceil_{odd} \tag{1}$$

In the formula, f_s enotes the system's sampling frequency, which is equal to the down-sample frequency of the input data, ranging from 10 to 100 Hz.

$\lfloor\cdot\rceil_{\text{odd}}$ indicates rounding to the nearest odd integer.

Using the moving average method, the trend estimate $\hat{T}[n]$ can be expressed as:

$$\hat{T}[n] = \frac{1}{W} \sum_{\kappa=n-\frac{W}{2}}^{n+\frac{W}{2}} x[\kappa] \tag{2}$$

Finally, the compensated observation $y[n]$ is obtained by subtracting the trend estimate $\hat{T}[n]$ from the original observation $x[n]$.

$$y[n] = x[n] - \hat{T}[n] \tag{3}$$

2.3.2 Adaptive Median Filtering Algorithm for Windows

An adaptive median filtering method based on local statistical characteristics is employed. The filter window size W_{median} dynamically adjusts according to the local signal-to-noise ratio (SNR), calculated as:

$$W_{median} = max(3, min(11, \lfloor 10SNR + 3 \rceil)) \tag{4}$$

The window size for median filtering is adapted based on the signal-to-noise ratio (SNR), a measure of noise intensity. The median value within a sliding neighborhood is calculated for each data point, with processing deliberately limited to points fully within the window to avoid edge artifact. This design ensures robust suppression of impulse noise and excellent retention of edge information, effectively safeguarding important signal characteristics throughout the smoothing process.

2.3.3 Local Trajectory Smoothing Algorithm

This method employs dynamic adjustment of smoothing intensity to achieve effective trajectory smoothing while preventing shape distortion caused by excessive smoothing. The smoothing factor is determined by the estimated local variance of the trajectory. A large variance value, indicating significant data variation, necessitates a stronger smoothing effect. Conversely, in regions with small variance, a weaker smoothing factor is assigned to retain the intricate details of the original trajectory.

The local smoothing factor α is calculated using the following formula:

$$\alpha = 1 - exp\left(-\sigma_{local}^2\right) \tag{5}$$

Where σ_{local}^2 represents the variance estimate of the local trajectory. The smoothed output value is calculated as the weighted average of the current observation and its neighboring points:

$$y[n] = (1-\alpha)x[n] + \frac{\alpha}{2}(x[n-1] + x[n+1]) \quad (6)$$

In dynamic systems, trajectory curvature plays a significant role in smoothing effects. Excessive smoothing may distort the trajectory shape. Therefore, this method flexibly adjusts the smoothing factor by analyzing local variance, ensuring effective noise suppression while preserving the trajectory's authentic features and structure.

2.3.4 Error Prediction Compensation Algorithm Based on AR Models

In addition to the frequency-based low-frequency error compensation described in Section 2.3.1, this paper adopts an error prediction method based on the autoregressive (AR) model to effectively reduce systematic errors. Historical error sequences are utilized to forecast future errors, with dynamic adjustments applied to compensate for systematic errors. The specific workflow is as follows:

Step1:

Calculate the error between the measured value and the true value at each time point to construct the historical error sequence. Then, model and predict the historical errors using a second-order AR model. The prediction formula is as follows:

$$\hat{e}[n] = \theta_1 e[n-1] + \theta_2 e[n-2] \quad (7)$$

The predicted values are composed of weighted historical errors, where θ_1 and θ_2 are model parameters calculated using exponentially decaying weights:

$$\theta_k = \frac{e^{-0.5k}}{\sum_{j=1}^{2} e^{-0.5j}} \{\kappa = 1,2\} \quad (8)$$

The kernel $e^{-0.5k}$ allocates greater informational weight to recent observations, naturally attenuating outdated prior errors. It ensures the system remains responsive to sudden legitimate trajectory shifts and prevents phase lag induced by pure historical predictions. This optimal balance significantly mitigates model mismatch while preserving dynamic tracking accuracy.

Step2:

To avoid overcompensation, the final compensation result is calculated as a weighted average of the predicted value and the current measured value, with 70% weight assigned to the predicted value and 30% to the current value:

$$y[n] = 0.7 \cdot \hat{e}[n] + 0.3 \cdot x[n] \quad (9)$$

This algorithm effectively balances the weights of predicted values and current observations, preventing performance degradation due to overcompensation.

2.3.5 Confidence-Weighted Truth Value Correction Algorithm

The confidence-weighted true value correction method specifically targets systematic bias and model mismatch errors. By multi-factor confidence assessment, it performs true value-weighted corrections to measured values. Specifically, it first calculates the correction confidence for each point, considering multiple factors including star point intensity (I), sub-pixel accuracy estimation (A), and the distance to reference true values (D). The confidence level (γ) is calculated as follows:

$$\gamma = max\left(0.1, min\left(0.9, \left(\frac{I}{100} + (1-10A)\right) \cdot \frac{1}{2} \cdot exp(-D)\right)\right) \quad (10)$$

Where

I represents the intensity of the measurement point, normalized to the range [0, 1];

A represents sub-pixel accuracy; smaller value of A indicate higher confidence. When sub-pixel interpolation is not used, A = 0;

D denotes the distance between the measurement point and the ground truth. The final confidence γ is constrained within the range [0.1, 0.9].

Measurement values (G) are weighted and compensated based on the confidence value and ground truth (M) using the following formula:

$$output = \gamma \cdot G + (1-\gamma) \cdot M \quad (11)$$

In this formula, G represents the original measurement value, M represents the true value, and the closer the measurement point is to the true value, the higher the confidence.

2.4 Adaptive Selection Mechanism for Error Compensation Strategies

Define the strategy matching score as the selection criterion, which takes into account factors such as the target error margin, compensation coefficient, strategy effectiveness, and strategy cost. The matching score is calculated using the following formula:

$$Score_j = \sum_k (A_{jk} \cdot C_{jk}) \times E_j \times (1 - D_j) \quad (12)$$

Where:

A_{jk}: the magnitude of error category k under strategy j,

C_{jk}: the compensation capability of strategy j for error category k,

E_j: the effectiveness evaluation value of the strategy,

D_j: the estimated execution cost of the strategy.

In aerospace applications, star trackers operate on embedded platforms with strictly limited computational resources. Therefore, algorithmic complexity is a critical constraint. The inclusion of the execution cost (D_j) in the matching score ensures that the system avoids blindly applying computationally expensive algorithms (such as complex matrix operations) to every frame. Instead, it dynamically balances the trade-off between accuracy improvement and computational burden. This adaptive allocation of computing power guarantees real-time processing capabilities at high sampling rates, such as 200 Hz and 300 Hz, without overwhelming the hardware.

Strategy Name	Effect Estimate (E_j)	Execution Cost (D_j)	Target Error Type
Adaptive Median Filtering Algorithm for Windows	0.7	0.3	SYSTEMATIC_LOW_FREQ
Adaptive Median Filtering Algorithm for Windows	0.6	0.2	SYSTEMATIC_HIGH_FREQ, MEASUREMENT_NOISE
Local Trajectory Smoothing Algorithm	0.5	0.1	RANDOM_QUANTIZATION, MEASUREMENT_NOISE
Error Prediction Compensation Algorithm Based on AR Models	0.8	0.4	MODEL_MISMATCH
Confidence-Weighted Truth Value Correction Algorithm	0.9	0.5	SYSTEMATIC_LOW_FREQ, MODEL_MISMATCH

Table 1

Compensation Strategy Parameter Configuration Table

Table 1 above summarizes the employed error compensation strategies along with their parameter configurations. The three strategies with the highest matching scores are selected and executed sequentially in descending order. Following the application of each strategy, its compensation effect is quantitatively evaluated. A compensation pass is reverted if its effect falls below a predefined threshold of 1%, which is set to gauge the strategy's contribution to measurement improvement. This step-wise, conditional execution ensures that only substantively effective compensations are retained. Here, $RMSE_{before}$ and $RMSE_{after}$ represent the error before and after compensation, respectively.

$$Effective = \frac{RMSE_{before} - RMSE_{after}}{RMSE_{before}} \tag{13}$$

After compensation, the centroid extraction sequence is updated to obtain the compensated results, and the root mean square error ($RMSE$) is calculated as the accuracy evaluation criterion. To ensure that the selected strategy effectively reduces errors, this paper employs a matching function to assess the compensation effectiveness of the strategy. The matching function M_{ij} is calculated based on the alignment between different error types and the compensation capability of the strategy. Its specific form is defined as:

$$M_{ij} = \frac{E_k \delta\left(T_i, C_{jk}\right) \cdot A_{jk}}{E_k A_{jk}} \tag{14}$$

In the formula, T_i denotes the error type, C_{jk} represents the compensation capability of the j-th strategy for the k-th error category, and A_{jk} is the error magnitude. The matching function synthesizes these factors to assess the adaptability of strategies and dynamically selects the optimal strategy combination for practical applications.

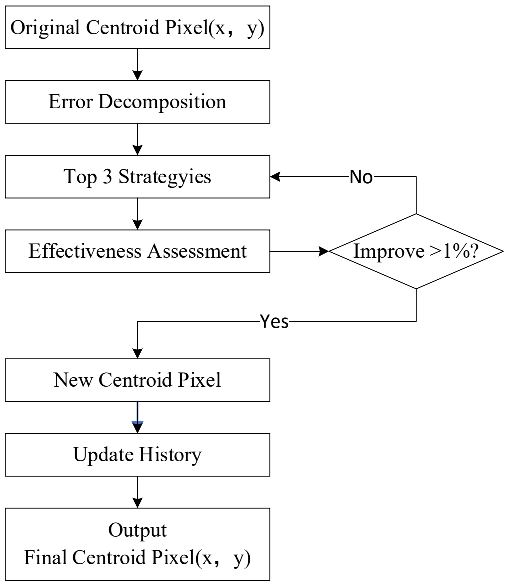

Figure 1 Compensation Algorithm Flowchart

Figure 1 presents an algorithmic flowchart for error compensation. This flowchart starts with the raw centroid sequence from the UKF, subjects it to error decomposition, and then sequentially applies the three top-ranked compensation strategies, wherein any strategy that yields an improvement of less than 1% is subsequently rolled back.

2.5 Evaluation Criteria

The root mean square error ($RMSE_i$) of the sequence centroid is used as the primary evaluation criterion to assess the accuracy improvement before and after compensation. The formula is as follows:

$$RMSE_i = \sqrt{\frac{1}{N}\sum_{i=1}^{N}[(x_i - x_{mean})^2 + (y_i - y_{mean})^2]} \quad (15)$$

For each star point i, calculate its deviation in the X and Y directions: $\Delta x_i = x_i - x_{mean}$, $\Delta y_i = y_i - y_{mean}$.

3. Experiment and Discussion

3.1 Experimental Data and Design

The experimental data consists of 3248 300Hz and 3027 200Hz laboratory-simulated star maps. Considering the bandwidth limitations of the uplink and downlink channels, original frame rate data is typically not used in practical applications. Instead, a down-sample frequency ranging from 10 to 100Hz with equidistant sampling intervals is applied.

Experimental Protocol:

First, center-of-mass sequences are extracted using five motion models with unscented Kalman filters across the two datasets, and the root mean square error ($RMSE$) is calculated. The motion model yielding the highest extraction accuracy is identified. Next, four sub-pixel interpolation methods are combined with the optimal motion model's unscented Kalman filter to extract center-of-mass sequences, which serve as input data for the error modeling and compensation method. The accuracy improvement of this method is validated when fixed to the selected motion model. Finally, the accuracy improvement is compared across different motion models.

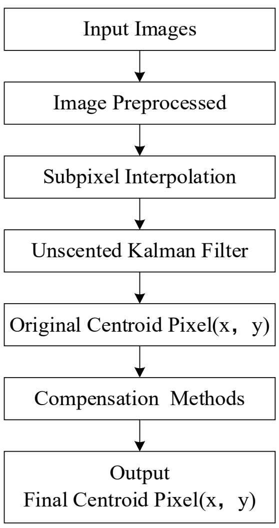

Figure 2 Experimental Flowchart

Figure 2 illustrates the complete workflow of the experiments in this paper. Figure 1 provides a detailed breakdown of the “Compensation Methods” shown in Figure 2.

3.2 Results Analysis

3.2.1 Motion Model Selection

Center-of-mass sequences are constructed from the datasets with original measurement frequencies of 300Hz and 200Hz using the method described in Section 2.1.

Sub-pixel Method	UKF Model	300Hz		200Hz	
		RMSE_5Hz	RMSE_10Hz	RMSE_5Hz	RMSE_10Hz
NONE	STATIC	0.4481	0.4374	0.3173	0.3230
	RANDOM_WALK	0.4683	0.4691	0.3914	0.3758
	BROWNIAN_MOTION	0.4683	0.4693	0.3912	0.3756
	POLYNOMIAL_TREND	0.4761	0.4759	0.3913	0.3941
	CONSTANT_VELOCITY	0.4761	0.4762	0.3826	0.3696

Table 2 Statistical Summary of Uncompensated Extraction Accuracy for Different Motion Model UKF Methods on Two Datasets

1. STATIC model

Suitable for ideal stable scenarios where the target is absolutely stationary or its positional fluctuation is far below the measurement precision.

2. RANDOM_WALK model

Appropriate for simulating position drift dominated by random disturbances without clear patterns.

3. BROWNIAN _MOTION model

Models the motion of a target under random force, where the noise is injected into the velocity component, resulting in a continuous but non-differentiable path. It is suitable for scenarios like particle diffusion in fluids or long-term drift of vehicles under environmental disturbances.

4. POLYNOMIAL_TREND model

Used to describe complex trending motion with slowly changing acceleration.

5. CONSTANT_VELOCITY model

The most universal basic model, applicable for tracking most targets with steady uniform motion.

As shown in Table 2, for both datasets with fixed down-sample frequencies of 5Hz and 10Hz. Among the five motion models above, the STATIC model performed the best, consistent with theoretical expectations. This is because the laboratory simulation of star chart data acquisition did not introduce any physical motion of the camera platform, only minor perturbations. Furthermore, as shown in Figure 3-(c), the discrete nature of the star points during imaging resulted in a root mean square error ($RMSE$) in the initial centroid extraction accuracy ranging from 0.31 to 0.45 pixels, leaving room for improvement.

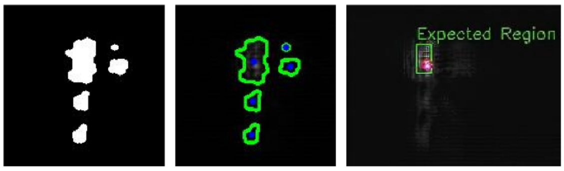

(a) (b) (c)

Figure 3 RMSE Statistics Before and After Error Compensation

Figure 3-(a)

It shows the binary image after foreground segmentation with thresholding, where white regions represent potential star point areas.

Figure 3-(b)

It displays the image of morphologically connected regions, with blue points indicating the initial centroid extraction positions calculated using image moments, which are then refined through second-order Gaussian fitting.

Figure 3-(c)

It illustrates the centroid extraction positions within a single image.

3.2.2 Experiment on Error Modeling and Compensation

(1) Optimal Motion Model Error Compensation Experiment

The experiment used a fixed motion model (STATIC). Four sub-pixel interpolation methods were employed to obtain coarse ground truth, followed by the extraction of initial center-of-mass sequences using the STATIC motion model's unscented Kalman filter. The mean of the entire initial center-of-mass sequence was selected as the ground truth. Error compensation experiments were conducted on the two datasets with down-sample frequencies of 10, 20, 30, 40, and 50 Hz. The experimental results are presented in the table below:

UKF Modle：STATIC			Truth Value：Full Stars Average			
Sub-Pixel Method	**Downs-ample Frequency/Hz**	**Image number**	**300Hz RMSE_Before**	**300Hz RMSE_After**	**200Hz RMSE_Before**	**200Hz RMSE_After**
NONE	10	60	0.4374	**0.1281**	0.3230	**0.3225**
	50	300	0.4529	**0.1364**	0.3408	**0.1547**
BICUBIC	10	60	1.7547	**0.1305**	1.5008	1.5008
	30	200	1.7655	**0.1339**	1.5380	**0.1548**
	50	300	1.7792	**0.1387**	1.5348	**0.1557**
GAUSSFIT	10	60	0.1034	0.1034	0.3627	**0.1517**
	50	300	0.1097	0.1097	0.1341	0.1341
GRADIENT	10	60	2.4485	**0.2068**	2.7714	**0.1834**
	50	300	2.5500	**0.1442**	3.0936	**0.1693**
MOMENT	10	60	0.9319	**0.1282**	0.9136	**0.1454**
	50	300	0.8988	**0.1373**	0.9203	**0.1548**

Table 3 Error Compensation for Various Sub-pixel Interpolation Methods in the STATIC Model

As shown in Table 3, across both datasets, the error compensation method showed significant improvements for the NONE, GRADIENT, and MOMENT sub-pixel interpolation methods, with post-compensation extraction accuracy exceeding 0.21 pixels. For the GAUSSFIT method, the improvement was modest, but the overall extraction accuracy still exceeded 0.16 pixels. For the BICUBIC method, centroid localization accuracy improved by over 90% across sample sizes ranging from 120 to 300, though the improvement was limited in the small-sample scenario with 60 data points.

Figure 4 presents detailed statistics on centroid extraction accuracy before and after error compensation for data with an original sampling frequency of 300Hz. This analysis uses a static motion model and four sub-pixel interpolation methods under down-sample frequencies of 10-50Hz (60-300 data points).

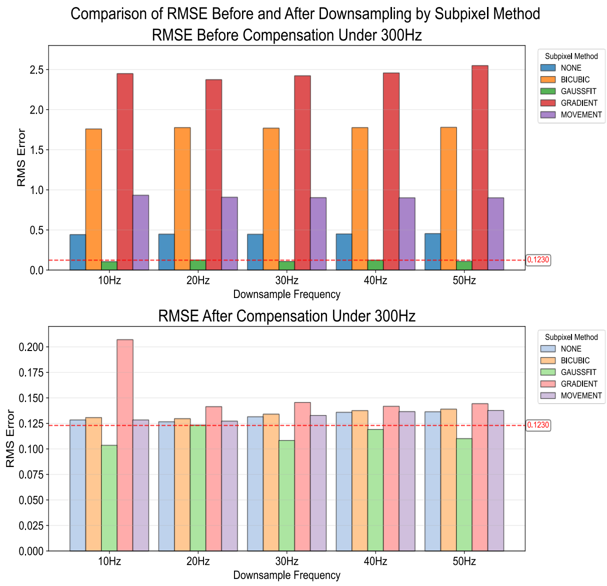

Figure 4 Statistical Bar Chart of RMSE Before and After Error Compensation

Experimental results confirm that the proposed error modeling and compensation method significantly boosts the centroid extraction accuracy for the STATIC unscented Kalman filter model. The evidence is twofold: First, without subpixel interpolation, accuracy was enhanced from 0.4452 to 0.1317 pixels. Second, when integrated with interpolation methods such as BICUBIC, GRADIENT, and MOMENT, the initial accuracies of 1.7702, 2.4499, and 0.9077 pixels were elevated to 0.1340, 0.1558, and 0.1323 pixels, respectively. The sole exception was third-order GAUSSFIT, where accuracy plateaued at 0.1126 pixels. This is because its inherent high precision, reflected in a post-interpolation accuracy of 0.076899 pixels, and the system's proximity to its theoretical limit after the unscented Kalman filter correction at 0.24439 pixels, left no room for further gains. Crucially, post-compensation accuracy consistently converged to a superior band of 0.11–0.16 pixels, a marked improvement over the initial 0.31–0.45 pixel baseline.

(2) Comparison of Multiple Motion Models

Sub-Pixel Method: NONE Truth Value: Full Stars Average Down-sample Frequency:50Hz				
UKF Model	300Hz RMSE_Before	300Hz RMSE_After	200Hz RMSE_Before	200Hz RMSE_After
STATIC	0.4529	**0.1364**	0.3408	**0.1544**
RANDOM _WALK	0.3860	**0.2870**	0.4843	**0.1931**
BROWNIAN _MOTION	0.4843	**0.1931**	0.3860	**0.2871**
POLYNOMI AL_TREND	0.4904	**0.1730**	0.4037	0.4023
CONSTANT _VELOCITY	0.4922	**0.1721**	0.3792	0.3766

Table 4 Error Compensation for Various UKF Motion Models

As shown in Table 4, based on the preliminary centroid e xtraction from the Kalman filter under five motion models, a comparative analysis of the centroid error before and a fter compensation was conducted at sampling frequencies o f 300Hz and 200Hz. The experimental results demonstrate that the proposed error compensation method effectively i mproves center-of-mass positioning accuracy across various motion models and sampling frequencies.

To further illustrate the applicability of this method at different sampling frequencies, the sampling range was extended to 10–100Hz, as shown in Figure 5 below.

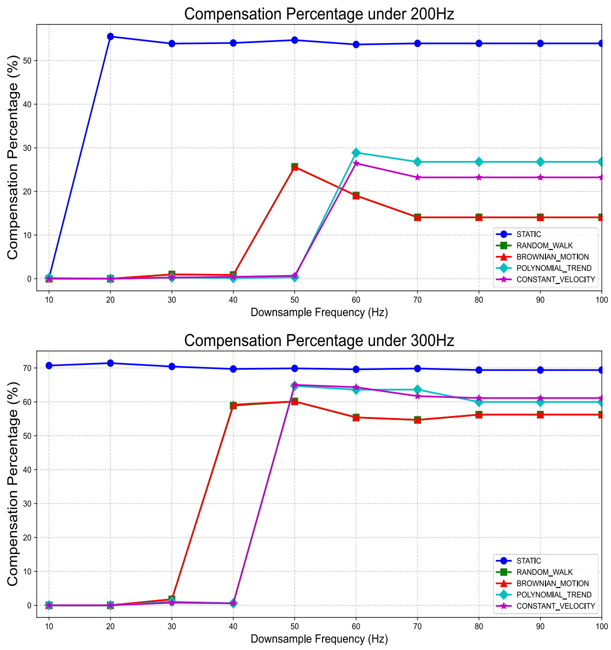

Figure 5 Compensation in the 200 and 300 Hz Datasets

The experimental results in Figure 5 demonstrate the broad applicability and robustness of the proposed error compensation method. It consistently improves centroid extraction accuracy for all five Unscented Kalman Filter (UKF) motion models, tested on simulated star image sets ranging from 30 to 600 samples. This performance gain stabilizes as the dataset grows, with the 300 Hz dataset showing particularly impressive results—accuracy improvements surpass 50% for sample sizes between 300 and 600. This successful validation across different models and sample conditions underscores the method's reliability in generating stable and high-precision centroid coordinates.

4. Conclusion

This paper addresses the error characteristics in star point centroid extraction by modeling and compensating for centroid extraction errors. It employs an adaptive window trend estimation algorithm to suppress systematic drift, uses a local trajectory smoothing algorithm and median filtering to eliminate high-frequency random errors, and corrects model mismatch through a confidence-weighted truth fusion correction algorithm and an error prediction compensation algorithm based on an AR model.

Experimental results demonstrate that the proposed method significantly enhances centroid extraction accuracy. On the 300 Hz and 200 Hz simulated star image datasets with a down-sample frequency of 10–50 Hz (corresponding to 30–300 images), the average accuracy was improved from 0.31–0.45

pixels to 0.11–0.16 pixels and 0.15–0.19 pixels, respectively. Notably, the method exhibited consistent adaptability across various motion models and sub-pixel interpolation techniques, thereby providing robust technical support for high-precision star sensor attitude determination.

Future research could further optimize the real-time performance of the strategy selection mechanism and reduce computational overhead to accommodate resource constraints on embedded platforms such as onboard real-time computing systems. Additionally, exploring the integration of error compensation methods with deep learning-based extraction models could further enhance centroid extraction accuracy in complex scenarios, such as those with low signal-to-noise ratios.

References

Bin, L., Hai-long, Z., Tao, Z. and Yu-chan, T., 2016. Research status and development tendency of star tracker technique. Chinese Optics, 9(1), pp.16-29. doi.org/10.3788/ CO.20160901. 0016

Delabie, Tjorven, Joris De Schutter, and Bart Vandenbussche. "An accurate and efficient gaussian fit centroiding algorithm for star trackers." The Journal of the Astronautical Sciences 61, no. 1 (2014): 60-84.

Jiang, J., Xiong, K., Yu, W., Yan, J. and Zhang, G., 2016. Star centroiding error compensation for intensified star sensors. Optics express, 24(26), pp.29830-29842. doi.org/10.1364/OE. 24.029830

Liebe, C.C., 2002. Accuracy performance of star trackers-a tutorial. IEEE Transactions on aerospace and electronic systems, 38(2), pp.587-599. doi.org/ 10.1109/TAES.2002.1008988

Luo, L., Xu, L. and Zhang, H., 2015. Improved centroid extraction algorithm for autonomous star sensor. IET Image Processing, 9(10), pp.901-907. doi.org/10.1049/iet-ipr.2014. 0488

Shortis, M.R., Clarke, T.A. and Short, T., 1994, October. Comparison of some techniques for the subpixel location of discrete target images. In Videometrics III (Vol. 2350, pp. 239-250). SPIE. doi.org/10.1117/12.189136

Sun, T., Xing, F. and You, Z., 2013. Optical system error analysis and calibration method of high-accuracy star trackers. Sensors, 13(4), pp.4598-4623. doi.org/10.3390/s130404598

Tan, W., Qin, S., Myers, R.M., Morris, T.J., Jiang, G., Zhao, Y., Wang, X., Ma, L. and Dai, D., 2017. Centroid error compensation method for a star tracker under complex dynamic conditions. Optics Express, 25(26), pp.33559-33574. doi.org/10.1364/OE.25.033559

Wang, D., Han, Y. and Sun, T., 2013, September. Star sub-pixel centroid calculation based on multi-step minimum energy difference method. In International Symposium on Photoelectronic Detection and Imaging 2013: Infrared Imaging and Applications (Vol. 8907, pp. 1420-1425). SPIE. doi.org/10.1117/12.2038813

Wei, X., Wen, D., Song, Z., Xi, J., Zhang, W., Liu, G. and Li, Z., 2019. A systematic error compensation method based on an optimized extreme learning machine for star sensor image centroid estimation. Applied Sciences, 9(22), p.4751. doi.org/10.3390/app9224751

Yu, W., Qu, H. and Zhang, Y., 2023. A high-accuracy star centroid extraction method based on Kalman filter for multi-exposure imaging star sensors. Sensors, 23(18), p.7823. doi.org/10.3390/s23187823

Zong, H., Gao, X., Wang, B., Wang, H. and Li, L., 2014. Method of star extraction on strong interference. Harbin Gongye Daxue Xuebao/Journal of Harbin Institute of Technology, 46(8), pp.113-117.